Soft Matter

PAPER

View Article Online
View Journal | View Issue

Cite this: *Soft Matter*, 2016, 12, 2729

Interaction dynamics of two diffusing particles: contact times and influence of nearby surfaces

B. Tränkle,[a] D. Ruh[a] and A. Rohrbach*[ab]

Received 21st December 2015,
Accepted 20th January 2016

DOI: 10.1039/c5sm03085d

www.rsc.org/softmatter

Interactions of diffusing particles are governed by hydrodynamics on different length and timescales. The local hydrodynamics can be influenced substantially by simple interfaces. Here, we investigate the interaction dynamics of two micron-sized spheres close to plane interfaces to mimic more complex biological systems or microfluidic environments. Using scanned line optical tweezers and fast 3D interferometric particle tracking, we are able to track the motion of each bead with precisions of a few nanometers and at a rate of 10 kilohertz. From the recorded trajectories, all spatial and temporal information is accessible. This way, we measure diffusion coefficients for two coupling particles at varying distances h to one or two glass interfaces. We analyze their coupling strength and length by cross-correlation analysis relative to h and find a significant decrease in the coupling length when a second particle diffuses nearby. By analysing the times the particles are in close contact, we find that the influence of nearby surfaces and interaction potentials reduce the diffusivity strongly, although we found that the diffusivity hardly affects the contact times and the binding probability between the particles. All experimental results are compared to a theoretical model, which is based on the number of possible diffusion paths following the Catalan numbers and a diffusion probability, which is biased by the spheres' surface potential. The theoretical and experimental results agree very well and therefore enable a better understanding of hydrodynamically coupled interaction processes.

1. Introduction

The evolution of life over billions of years has been accompanied by many safety mechanisms.[1] The simplest of these control mechanisms is based on a multitude of interactions between cellular components or between molecules, which act on specific short ranges and unspecific long ranges, but also on different time-scales. Among the long-range interactions hydrodynamic interactions play a superordinate role, since they affect the interaction dynamics between small particles in close vicinity, as *e.g.* through the viscosity of the surrounding fluid. In this way, the interaction probability between two binding particles can be strongly reduced, if the arrival of one particle is delayed at the interaction site. Living cells vary the size of their compartments and the distance to interfaces such as membranes and thereby change the local viscous drag.[2]

A typical strategy to better understand these mechanistic principles, is to mimic cellular systems or colloidal solutions and to reduce their complexity. A popular mimetic system consists of a few diffusing colloids in a controllable external potential, where the diffusion coefficients of one or two coupled spheres can still be determined experimentally and theoretically.[3,4] The motion of colloidal particles such as micron-sized spheres can be measured and manipulated with optical tweezers and position tracking techniques.

In this way, the hydrodynamic coupling of two particles was investigated by means of two adjacent static optical traps.[5,6] Here, position correlation functions turned out to be a versatile analysis tool to gain insights into hydrodynamic coupling. Optical traps were also used to induce colloidal interactions and to investigate the influence of nearby surfaces.[7–10] The tracking of the colloids translational motion allows to determine interaction parameters such as relative diffusion coefficients and inter-particle contact times. In this context, the influence of nearby cell membranes on the particle motion were measured by means of magnetic[11] and also optical tweezers.[12]

The diffusion inside small artificial vesicles was investigated[13] using video microscopy, which is still the standard particle tracking technique, although it is rather slow and erroneous in axial direction. Until now, there have been only very few studies, investigating the interaction of several particles influenced by nearby surfaces.[10,14–16] A second nearby surface was only investigated for single diffusing particles or by bulk measurements.[17,18] The influence of further boundaries was theoretically described by a linear superposition principle.[19]

[a] *Department of Microsystems Engineering (IMTEK), University of Freiburg, 79110 Freiburg, Germany. E-mail: rohrbach@imtek.de*
[b] *BIOSS Centre for Biological Signalling Studies, University of Freiburg, 79104 Freiburg, Germany*

Experimentally it is far from trivial to determine the 3D positions of many diffusing particles on short timescales. Back focal plane (BFP) interferometry is not only a precise and fast 3D tracking technique for a single particle,[20] it can also be used for several particles in an extended single optical potential[21,22] or in an array of optical point traps.[23] In this way the hydrodynamic interaction of two microspheres touching each other in a single optical potential could be investigated on a time window between 100 μs and 2 s.[22]

Although several novel tracking techniques have emerged, none of them has been applied to investigate how interfaces influence the hydrodynamic coupling and the contact times of two diffusing particles touching each other. How quickly do relative modes of motion decay, how is the diffusion coefficient influenced or how is the distribution of contact times altered by the interface?

These questions are addressed in our paper, which is organized as follows: first, we analyse the motion of two particles in a single potential with respect to their contact times and put this in the context of a mathematical framework, which helps to explain the observed contact time distributions. In the second part we study the coupling of two particles diffusing in a single potential nearby one and two flat glass interfaces.

Experimental principle of investigation

In our approach, we use an extended, line-shaped optical potential, also called a line optical trap to trap two silica-microspheres (radius $a \approx 489$ nm, Bangs labs, size variation 10–15%) in the same optical potential. The extended optical potential is generated by scanning a optical point trap at 10 kHz in a unidirectional manner (see ref. 21 and 22 for details). The extended optical trap allows the particles to diffuse in all three directions, where the weakest confinement (several micrometer) of the optical trap is in the scanning direction x, while in the perpendicular directions y and z the particles motions are much stronger confined, with estimated fluctuation widths $\Delta x = 36$ nm and $\Delta z = 115$ nm (see Fig. 1). While scanning the laser focus, light is scattered at the particles and interferes with unscattered light. The interference intensity is projected onto two quadrant photodiodes,[21,24] which are used to determine the particles positions in 3D with nanometer precision and at sub-millisecond time resolution.[22,25]

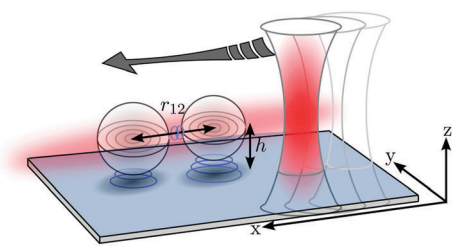

Fig. 1 Experimental scheme to investigate hydrodynamic coupling. The laser focus is scanned fast in one dimension to generate a line optical trap. The trapped particles diffuse rather freely in x-direction, but are confined in y- and z-direction. The spheres diffusivities are influenced by nearby surfaces and mutual hydrodynamic coupling (indicated by the blue circles).

To study the impact of nearby surfaces outlined in Fig. 1, we used the piezo stage to alter the spheres' position with respect to one or two horizontal flat interfaces. This was achieved by confining the spheres in a chamber consisting of two opposing coverslips. The samples were prepared using a small coverslip, placed on top of a bigger coverslip. The height of the chamber was roughly controlled by the volume of the colloidal solution brought in between the two plates. To avoid fluid flow and evaporation, the chamber was sealed with vacuum grease. The height $L \approx 7$ μm of the chamber was measured as follows. While trapping a colloid in the optical trap, the chamber was moved stepwise in axial direction using a piezo stage. For a sphere center height $h \approx a$ and for $h \approx L - a$, the sphere was displaced from the center of the trap by the coverslip surfaces. The axial displacement was precisely recorded using BFP-interferometry, with a spatial resolution of 3–5 nm. The distance between the two points where the mean axial particle position begins to shift from of the trap center yields the chamber height $L + 2a$.

2. Theoretical framework

2.1 Distribution of contact times

The diffusive behavior of a Brownian particle is often modeled *via* a stochastic driving force, resulting in stochastic variables for the particles' degrees of freedom. Since for contact events between particles only the interparticle distance r_{12} is decisive, we can describe the occurrence of contact events by a single stochastic position variable in relative coordinates $r_{12}(t)$ (see Fig. 1). For each time step, this distance variable increases or decreases randomly by Δd. If r_{12} falls below the threshold distance R_0, a contact is assumed to be possible and the time $\tau_{on} = \tau_{end} - \tau_{start}$ is measured (blue trajectories in Fig. 2).

In our model, the start of a contact process is depicted by the green point in Fig. 3, where the number of paths, which lead to a certain grid point (*i.e.* a position sample point) is indicated by the black numbers above the paths shown in Fig. 3. The number of possible return paths (random walks) that lead out of the contact zone after n steps, is given by the number series 1, 1, 2, 5, 14,...(red numbers in Fig. 3). As it turns out, this series is well known for diffusive processes and in game theory and is given by the so called Catalan numbers $C(n)$.[26]

$$C(n) = \frac{(2n)!}{(n+1)!n!}. \quad (1)$$

The total number of possible paths after n time steps is $Z(n) = 2^{2n}$ (green numbers in Fig. 3), since there are always two possible directions and the contact zone can only be left after an even number of substeps $2n$. Therefore, the probability to find a path of length n which has never left the contact zone is given by

$$P(n) = \frac{C(n)}{Z(n)} = \frac{(2n)!}{(n+1)!n!2^{2n}} \quad (2)$$

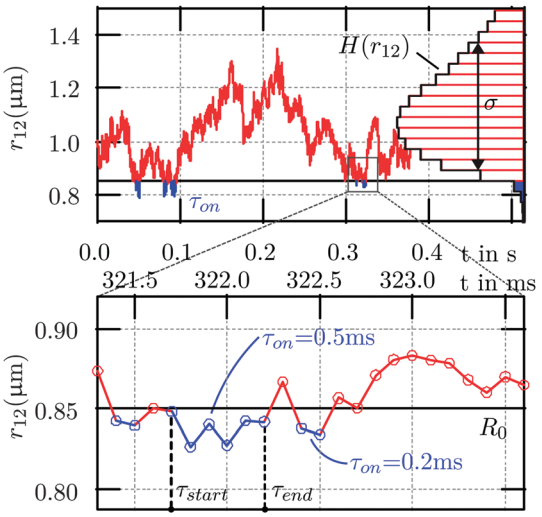

Fig. 2 Interparticle distance trajectory and distance histogram. Determination of contact times τ_{on} for two particles in a single potential: the interparticle distance r_{12} is determine by the 3D trajectories $\boldsymbol{r_1(t)}$ and $\boldsymbol{r_2(t)}$. Each time r_{12} falls below a threshold distance R_0, the time τ_{on} is counted.

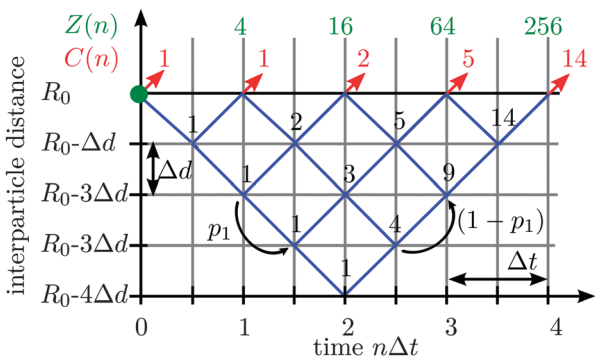

Fig. 3 Schematic illustrating the Catalan numbers. The diffusion pathways after n time steps Δt can be modeled by a stochastic variable r_{12}. The number of possible paths to each knot is counted by the numbers above. Starting at $r_{12} = R_0$, there is a single path leaving the contact zone after $n = 1$ time step and overall $Z = 4$ possible paths. After $n = 3$ time steps there are $C = 5$ leaving paths and altogether $Z = 64$ possible paths.

Using the Stirling equation[27] $n! \simeq \sqrt{2\pi n}\left(\frac{n}{e}\right)^n$ for $n \to \infty$, one finds

$$P(n) \simeq \sqrt{\frac{1}{\pi}} n^{-3/2}. \quad (3)$$

Since we did not make any constrictions to the minimal time step Δt, this approximation holds valid for sufficiently fast sampling $\propto 1/\Delta t$, or long contact times $\tau_{on} = n{\cdot}\Delta t$. In this case, the overall behaviour of $P(n)$ is well described by a power law with exponent $\alpha = -3/2$.

For two colloidal particles in a single potential, a further interaction potential V has to be taken into account. Electrostatic repulsion between the spheres leads to a shift in the stepping probability for steps towards or out of the contact zone. In terms of first return probabilities this effect has been modeled using different probabilities for steps back and forth by Wan *et al.*[28] If the probability for one substep is denoted by p_1 and a substep in reverse direction by $(1 - p_1)$ (see Fig. 3), the contact time distribution in eqn (3) has to be expanded by an additional term[28]

$$P(n, p_1) \propto n^{-\frac{3}{2}} \cdot (4p_1(1-p_1))^{\frac{n}{2}}. \quad (4)$$

For a return of r_{12} to R_0 and without interaction potential, *i.e.* $V = 0$, positive and negative substeps occur with $p_1 = 1/2$ and equally often, namely n times. If however $p_1 \neq 1/2$, this will lead to an even faster decay of $p(n)$ on long timescales. In other words, a repulsive potential $V(r_{12})$ leads to a smaller probability for long contact times according to

$$P(\tau_{on}, p_1(V)) \sim \tau_{on}^{-\frac{3}{2}} (4p_1(V)(1-p_1(V)))^{\frac{\tau_{on}}{2}}. \quad (5)$$

Here, the one step probability $p_1 = p_1(V(R_0))$ depends on the force, *i.e.* the slope $\frac{\partial}{\partial r_{12}} V(r_{12})$ of the interaction potential at a defined distance $r_{12} = R_0$. The potential $V(r_{12}) = -kT{\cdot}\ln(H(r_{12})) + V_0$ can be derived by Boltzmann statistics from the interparticle distance histogram $H(r_{12})$ (see Fig. 2). The steeper the repulsive surface potential $V(r_{12})$, the larger is the repelling force $F(r_{12}) = -\frac{\partial}{\partial r_{12}} V(r_{12})$. In the case the particles can get into contact with each other at $r_{12} = 2a$ and experience a maximum repulsive surface force F_{max}, a straightforward way to express the forward step probability is given by

$$p_1(V(r_{12})) \approx \frac{1}{2}(1 - F(r_{12})/F_{max}) \approx \frac{1}{2}\left(1 - \frac{1}{F_{max}} \frac{\partial}{\partial r_{12}} \ln(H(r_{12}))\right). \quad (6)$$

For a repulsive, *i.e.* a decaying potential $V(r_{12})$, the probability for one forward step $p_1(V(r_{12}))$ becomes smaller until $p_1 = 0$ at the mechanical contact point $r_{12} = 2a$. With decreasing $p_1(V)$, longer contact times are significantly suppressed.

By averaging the contact time distribution $P(\tau_{on})$ over the whole measurement time T_{mes}, the association constant k_A is obtained: $k_A \approx \frac{1}{T_{mes}} \int_0^{T_{mes}} P(\tau_{on}) d\tau_{on}$. k_A is the average time, the particles are in contact relative to the total measurement time $T_{mes} = \sum(\tau_{on} + \tau_{off})$. As illustrated in Fig. 2 in blue colors, k_A can also be obtained from the distance distribution $H(r_{12})$.

In our experiments, we measure contact times $\tau_{on} = n{\cdot}\Delta t$ in seconds, which are multiples of the minimal sampling time $\Delta t = (10\ \text{kHz})^{-1} = 0.1$ ms.

2.2 Diffusion coefficients nearby surfaces

The motion of particles in a fluid are coupled *via* the hydrodynamic flow field. For two particles in external potentials with fixed distances it was shown, that this coupling results in an anti-correlated behavior of the particle fluctuations, *i.e.* their position cross-correlation function $C_x^c(\tau)$ in x direction is negative.[6,29] This characteristic could be explained by the difference in diffusion coefficients for collective and relative particle motion.[5] These findings could be extended by us experimentally to the diffusion

of two particles in a single potential and theoretically by the incorporation of an additional surface force.[22] In our present study, we introduce nearby surfaces in addition, which slow down the particle fluctuations.

The diffusion coefficients derived for a single particle moving parallel to a single surface is given by[19,30]

$$D_{\parallel}(h) = D_{\parallel 0}\left(1 - \frac{9}{16}\left(\frac{a}{h}\right) + \frac{1}{8}\left(\frac{a}{h}\right)^3 - \frac{45}{256}\left(\frac{a}{h}\right)^4 - \dots\right), \qquad (7)$$

where $D_{\parallel 0}$ is the diffusion coefficient far from the interface. The influence of a single surface on the diffusion coefficients of two particles with fixed distances was studied by Dufresne *et al.*[10] They found that a flat surface leads to a drop in both, relative and collective diffusion coefficients, D^{r} and D^{c}

$$D_{\parallel}^{\mathrm{c,r}}(r_{12}, h) = 2D_{\parallel 0}\left(1 - \frac{9}{16}\frac{a}{h} \pm \frac{3}{4}\frac{a}{r_{12}}\left[1 - \frac{1 + \frac{3}{2}4h^2/{r_{12}}^2}{(1 + 4h^2/{r_{12}}^2)^{\frac{3}{2}}}\right]\right) \qquad (8)$$

The plus-sign between the second and third summand corresponds to collective, the minus-sign to relative particle motion. The influence on the collective particle motion turns out to be more pronounced. For a decreasing distance to the surface $h \geq 0$, the interparticle contribution (third summand) tends to zero and D^{r} and D^{c} become indistinguishable. The diffusion coefficient, both for parallel and perpendicular movements of a particle enclosed in a chamber with height L and distance h to one of the surfaces can be described as[19]

$$D^{-1}(h,L) = D^{-1}(h) + D^{-1}(L - h - 2a) - {D_0}^{-1}. \qquad (9)$$

The first term on the right hand side of eqn (9) describes the first surface, the subsequent term the second surface, and the last term prevents to weight the free diffusion coefficient D_0 twice. In other words, this approach independently superposes the wall drag effects arising from each wall.

A theory describing the relative and collective diffusion coefficients of two particles in a chamber is so far not available. As a first estimation, one can apply the superposition principle shown in eqn (9) using the relative and collective diffusion coefficients in eqn (8). Here, one has to keep in mind that this leads to an overestimation of the mutual hydrodynamic coupling, *i.e.* the difference in D^{c} and D^{r}. This is because the superposition not only takes into account the second surface, but also includes again the correction terms for D^{c} and D^{r}. Although a simple superposition leads to twice the interparticle coupling, this approach can give a first impression of particle dynamics in confined volumes.

3. Experimental results

3.1 Distribution of measured contact times

The 3D position fluctuation data of two particles diffusing in a single potential was used to investigate their contact dynamics. In contrast to ensemble measurements, where the readout usually consists of the ratio of educts and products, line optical traps allow to check contact processes of single particles. The interparticle potential of the used particles is mainly determined by electrostatic repulsion. Therefore, irreversible bonds do not take place and contact processes can be investigated with high repeatability in a single measurement. The contact times were determined as sketched in Fig. 2. We first obtained the interparticle distance through $r_{12}(t) = |\boldsymbol{r_1(t)} - \boldsymbol{r_2(t)}|$. Subsequently, we scanned $r_{12}(t)$ for those trajectory parts, where $r_{12}(t)$ is throughout smaller than the threshold distance R_0 (blue trajectories in Fig. 2). All trajectory parts with the same duration τ_{on} were summarized and diagrammed in the distribution $P(\tau_{\mathrm{on}})$ (see Fig. 4a). In Fig. 4a, the predicted decrease in $P(\tau_{\mathrm{on}})$ for higher contact durations is clearly visible (the curves were normalized to contacts/second). The contact times of the same trajectory were determined for 3 different threshold distances R_0. These characteristic distances are displayed in Fig. 4b, where the interparticle histogram $H(r_{12})$ reveals the repulsive interaction for small distances. For higher values of r_{12}, $H(r_{12})$ drops again due to the optical potential, which confines the diffusion volume of both spheres. In good approximation, repulsive and attractive forces cancel out at the potential minimum, *i.e.* close to R_0 = 1.05 μm where the histogram is maximal. According to our model, the interparticle distance r_{12} decreases or increases at R_0 = 1.05 μm with the same stepping probability $p_1 = (1 - p_1) = 1/2$. In this case, a scale free power law was deduced with the exponent $\alpha = -3/2$, derived by the Catalan numbers $C(n)$. The same exponent $\alpha = -3/2$, can be measured by the blue line in Fig. 4a, which fits very well to the experimentally found data (blue symbols). By varying R_0 we can estimate the influence of the interaction potential $V(r_{12}) = -kT\cdot\ln(H(r_{12})) + V_0$ on the single step probability p_1 and thereby on $P(\tau_{\mathrm{on}},R_0)$. The green and red symbols correspond to contact durations with a smaller contact zone. The increase in $V(r_{12})$ can be described by a decrease in p_1. The lines in Fig. 4a correspond to eqn (5) with probabilities $p_1(R_0 = 0.95\ \mu\mathrm{m}) = 0.465$ and $p_1(R_0 = 0.88\ \mu\mathrm{m}) = 0.4$ respectively. As predicted, a higher repulsive potential leads to a steeper decrease in $P(\tau_{\mathrm{on}},p_1)$.

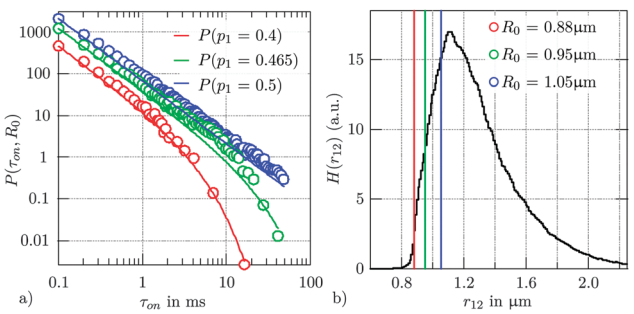

Fig. 4 Distribution of contact times and interparticle distance. (a) The frequency of contact times decreases for longer contact times. Experimental data is shown with markers for several threshold distances R_0. Theoretical data (shown with lines) corresponds to eqn (5) with step probabilities p. (b) Histogram of interparticle distances $H(r_{12})$ with threshold distances R_0 marked in coloured lines. The three distances R_0 correspond to three different strengths of the repulsive surface potential.

4. Hydrodynamic coupling to nearby surfaces

As predicted by eqn (7) and (8), the diffusion $D_\parallel(h)$ of a single particle, but also the relative diffusion $D^r_\parallel(r_{12},h)$ of two adjacent particles nearby a surface is slowed down due to an increased viscous drag. Therefore one may ask how this change in diffusivity influences the distribution $P(\tau_{on},h)$ of the contact times, the correlation between their position fluctuations, but also the diffusion of one particle close to another one and close to the surface.

4.1 Contact times between particles nearby surfaces

In the experiments, the mean distance $\langle h\rangle$ of the particles to the wall was varied by steering the height h_p of the piezo table. The contact time distribution $P(\tau_{on},h)$ was determined for 3 distinct distances h. Interestingly, the influence of the nearby surface on the contact time distribution is insignificant as shown in Fig. 5. This underlines the scale free formalism in eqn (3), which does not depend on time or local changes in diffusion coefficients. For short contact times, the power law is clearly visible (see Fig. 5a).

For sake of clarity, we summed all contact events in a certain time window (bars in Fig. 5a) and depict $P(\tau_{on},h)$ in the first time window of 0.1–1 ms in Fig. 5b. For smaller distances h, short contact processes occur slightly less often at higher viscosity. Since the sum of all contact times is determined by $H(r_{12})$, longer contact times occur more often.

4.2 Diffusion coefficients near surfaces

For the determination of the diffusion coefficients we calculated the autocorrelation function $C^a_i(\tau) = \langle \boldsymbol{r_{i1}}(t),\boldsymbol{r_{i2}}(t+\tau)\rangle$ of the particle trajectories $\boldsymbol{r_{ij}}(t)$, (j = 1, 2, i = x, y, z). On short timescales the particle does not see the potential and the diffusion coefficients are proportional to the slope of the autocorrelation function, $C^a(\tau) \approx -D{\cdot}\tau$. Fig. 6 shows the result of this analysis for a single bead diffusing parallel to a coverslip (x-direction) at a distance h (Fig. 6a) or between two coverslips (Fig. 6b). In Fig. 6a the curves are each normalized by their corresponding diffusion coefficients D_0 determined far from the coverslip surface (~40 μm), where hydrodynamic coupling to the surface can be neglected in good approximation. The theoretical prediction of eqn (7) is depicted by the solid red line.

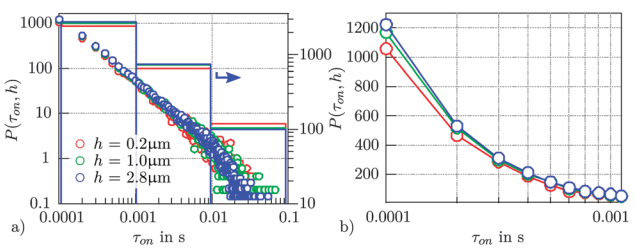

Fig. 5 Influence of nearby surfaces on the interaction probability. (a) Contact time distribution $P(\tau_{on},h)$ of two particles in a single potential up to τ_{on} = 100 ms. The distance h of the optical trap to the surface was stepwise decreased. The bars represent the sum over all contact events in the indicated time window. (b) Inset of $P(\tau_{on},h)$ for short contact times up to τ_{on} = 0.1 ms.

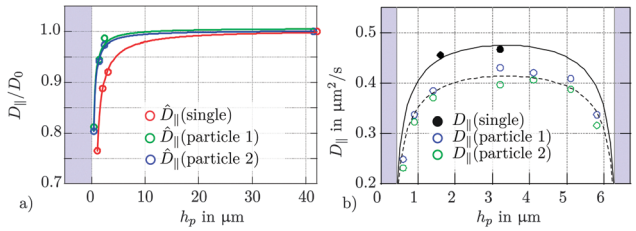

Fig. 6 Single particle diffusion coefficients in the vicinity of one or two surfaces. The regions inaccessible to the spheres due to the plane glass walls are shaded blueish. Their positions were determined using eqn (7) and (9). (a) Diffusion coefficients $D_\parallel(h)$ as a function of distance h from the interface for a single particle with and without a nearby particle. Solid lines correspond to a fit of eqn (7). (b) $D_\parallel$ for one and two particles between two flat surfaces. The solid lines were calculated using eqn (9). The thickness of the chamber was $L \approx 7$ μm.

The very same experiments were carried out with a second particle nearby (green and blue symbols in Fig. 6a). Here, the diffusion is not only hindered by the nearby wall but also influenced by the diffusion of the other particle in the same optical trap. For colloidal suspensions, it was shown that an increase in particle density leads to a drop of the self diffusional coefficient.[31] Furthermore, time multiplexed optical traps were used to study the influence of next neighbour particles in a 3 × 3 grid of trapped colloids.[23] As expected, a second nearby particle leads to a decrease in the single particle diffusion coefficient. Far away from the surface, we find a drop in D_0 by 17%.

For particles in the midplane between two walls, the sphere's diffusivity is suppressed near either wall (see Fig. 6b, black symbols correspond to a single particle in the trap, blue and green symbols to the diffusities for two particles in the same trap). A nearby particle leads to a drop in D_0 of about 15%. However, the qualitative behaviour of $D(h)$ close to surfaces does not change. As shown by the blue and green solid lines in Fig. 6a and the black dotted line in Fig. 5b, the course of $D(h)$ is well reproduced by eqn (7) and (9). A nearby particle leads to a decrease of the diffusion coefficient D_0 of 15%. A hydrodynamic decay length Λ can be defined by fitting an exponential such that $D(r_{12},h) \approx a{\cdot}\exp(-h/\Lambda(r_{12})) + b$. According to these fits, the coupling lengths $\Lambda(r_{12})$ decrease by a factor of about 3 for small r_{12} relative to $r_{12} \to \infty$ (single particle).

4.3 Relative and collective diffusion of two particles. After calculating the relative and collective position coordinates of the two particles, we determined the corresponding diffusivities D^r and D^c. As shown in Fig. 7a, the decrease of both, D_c and D_r near a flat surface is clearly visible. This drop is well reproduced by eqn (8), which is fitted to the experimental data (circles) and is shown by solid lines. During a measurement, the interparticle distance r_{12} is not constant, but changes continuously. For the mean value r_{12} or $D(r_{12})$, respectively, the differing values for $D(r_{12})$ were weighted using the histogram of the relative distance $H(r_{12})$ (see Fig. 4b). The distance dependent diffusivity inside a chamber has a symmetric course of D_r and D_c. The linear

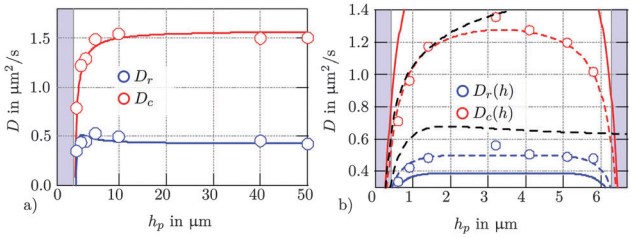

Fig. 7 (a) Relative and collective diffusion coefficients of two particles in the vicinity of one or two surfaces. Collective and relative diffusion coefficients of two colloids are plotted in red and blue, respectively. Circles represent experimental data, lines belong to theoretical predictions. The regions inaccessible to the spheres due to the plane glass walls are shaded blueish. (a) Single flat surface: solid lines correspond to eqn (8). (b) Two flat surfaces: Solid lines were calculated by eqn (9). Black dotted lines represent the theoretical course of D for a single surface according to eqn (8). Dashed lines: course given by eqn (9) with r_{12} = 2.5 μm (blue) and r_{12} = 1.5 μm (red). The thickness of the chamber was $L \approx 7$ μm.

superposition approximation made in eqn (9) leads to an overestimation of the mutual hydrodynamic coupling, *i.e.* the prediction yields to low values for D_r and to high values for D_c (straight lines). For comparison, the theoretical curves for a single surface are drawn in black dashed lines. This overestimation can be visualized by choosing a higher mean distance $\langle r_{12} \rangle$ of the spheres and thus lowering the contribution of mutual hydrodynamic effects between the spheres. The dashed lines correspond to a mean distance of $\langle r_{12} \rangle$ = 2.5 μm (blue) and $\langle r_{12} \rangle$ = 1.5 μm (red), respectively.

5. Influence of nearby surfaces on the interaction dynamics

The position fluctuations of two diffusing particles (index $j = 1, 2$) are stochastic, but correlated. The hydrodynamic coupling of their diffusive motion can well be seen in the cross-correlation $C_i^c(\tau) = \langle \boldsymbol{r_{i1}}(t), \boldsymbol{r_{i2}}(t + \tau) \rangle$ of the trajectories $\boldsymbol{r_{i1}}(t)$ and $\boldsymbol{r_{i2}}(t)$ ($i = x, y, z$).[5,6,23] For a better comparison, it is useful to normalize the function $C_i^c(\tau)$ by the particles standard deviation, which leads to the normalized correlation function $\hat{C}_i^c(\tau)$.

The theoretical course of $C_i^c(\tau)$ for two particles with fixed distance in two external potentials was predicted by Meiners *et al.*[29] For two particles in a single potential the correlation function is depending on short range interaction forces in addition.[22,32] The course of C_i^c is then determined by the acting surface forces and the difference in relative and collective diffusion coefficients.[22]

$$C_i^c(\tau, h) = \frac{k_B T}{2}\left(\frac{1}{\kappa_i} e^{-\frac{\kappa_i D_c(h)}{k_B T}\cdot\tau} - \frac{1}{(\kappa_i + \kappa_{is})} e^{-\frac{(\kappa_i+\kappa_{is})D_r(h)}{k_B T}\cdot\tau}\right) \quad (10)$$

Here, κ describes the optical trap stiffness, κ_s is the force constant describing the strength of the linear surface force, and $D_{c,r}(h)$ are the distance dependent diffusion coefficients of collective and relative motion.

As shown in Fig. 7, the diffusivities $D_{c,r}$ are reduced in the vicinity of surfaces and therefore we expect an influence on the

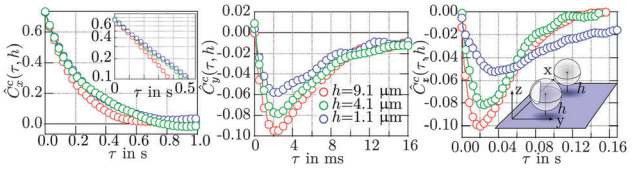

Fig. 8 Position cross-correlation functions for fluctuations parallel to the surface. The distance to the nearby surface was decreased stepwise. (a) A stepwise decrease of the distance h leads to a slower decrease in $\hat{C}_x^c(\tau)$. (b and c) For smaller distances h, the dip in $\hat{C}_y^c(\tau)$ and $\hat{C}_z^c(\tau)$ becomes less pronounced.

particle correlation functions. Fig. 8 displays the normalized cross-correlation functions $\hat{C}_i^c(\tau)$ of two particles in a single potential in all 3 dimensions ($i = x, y, z$). The distance to the surface was lowered by altering the glass surface h_p *via* the piezo stage. Corresponding to our previously obtained results,[22] the correlation function remains positive in the x-direction, since mutual surface forces dominate the spheres' motion. The particles predominantly move in the same direction (pronounced collective motion), favored by the electrostatic force. In other words, the relative (surface and optical) potential is steeper than the collective (optical) potential, leading to higher fluctuation widths in collective direction. In y- and z-direction, the surface force is less dominant and the potentials are approximately equal. Since relative position fluctuations decay faster than collective fluctuations due to the lower relative diffusivity, $\hat{C}_i^c(\tau)$ shows a negative slope according to eqn (10).[22]

As shown before, a nearby surface reduces both D_c and D_r. Therefore, $\hat{C}_i^c(\tau)$ in x-direction shows a slower decay. However, the decrease in $D(h)$ is steeper for relative motion than for collective motion. If r_{12} tends to infinity and h becomes minimal ($h \to a$), the hydrodynamic coupling to the surface is much stronger than the coupling between the spheres. A major benefit of using linetraps is that we can measure correlations effects in a timeframe of up to 2 s.

The effect, that a plane surface nearby two particles suppresses the hydrodynamic coupling, can be well seen in the correlation curves $\hat{C}_y^c(\tau)$ and $\hat{C}_z^c(\tau)$ of Fig. 8. The depth of the dips in $\hat{C}_y^c(\tau)$ and $\hat{C}_z^c(\tau)$ are expected to become smaller for decreasing distances h to the surface.

The two particle diffusion experiments in the chambers (two plane surfaces) underline the results found for a single flat surface. As displayed in Fig. 9, we observed a symmetric dependency of C_i^c ($i = x, y$) on the distance to one of the two surfaces. Again, the diffusion coefficients decrease and lead to a slower decay in $\hat{C}_y^c(\tau)$, whereas in y-direction, the negative values in $\hat{C}_z^c(\tau)$ become less pronounced. The maximal amplitude of the cross-correlation functions is significantly reduced by the influence of the surface.

6. Discussion

It remains an open question how interfaces influence the hydrodynamic coupling and the contact times of two diffusing particles touching each other. How quickly do relative modes of

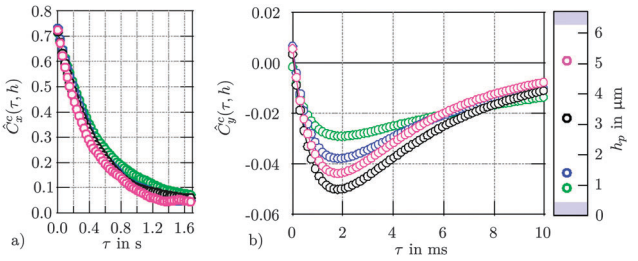

Fig. 9 Position cross-correlation function for two particles at two nearby surfaces. The fluctuation data was recorded at different distances of the line optical trap with respect to the surfaces. These positions relative to the surfaces are indicated by the colored markers on the right. (a) Cross-correlation function $\hat{C}_x^c(\tau)$ in scanning direction x. (b) Cross-correlation function $\hat{C}_y^c(\tau)$ in lateral y-direction.

motion decay, how is the diffusion coefficient influenced or how is the distribution of contact times altered by the interface?

The principle of investigation

The technique we used for the hydrodynamic particle coupling *via* interfaces was a combination of an optical line trap together with 3D back focal plane interferometry and had been introduced in our recent papers.[22,23] The presence of one or two horizontal glass interfaces had no influence on the 3D tracking precision, which will be likely not the case for additional vertical interfaces. However, the glass interfaces pushed the diffusing particles upwards in z-direction, which led to a reduced fluctuation volume. This stiffness of the optical trap in x- and y- direction, was not affected by the reduced z-fluctuations. Moreover the distance L between both interfaces needs to be varied in future experiments.

Distribution of contact times and interparticle distances

We could show that the Catalan numbers, which describe the number n of defined paths out of a defined volume, can be identified as a distribution of contact times $\tau_{on} = n{\cdot}\Delta t$ between two diffusing spheres for a defined threshold distance R_0. R_0 is typically some nanometers larger than the sum of the radii spheres (here 2a). For a diffusion without external forces or potentials, the probability to find the two particles within the contact distance over the time period τ_{on}, $P(\tau_{on},p_1) \sim \tau_{on}{}^{-3/2}(4p_1(1-p_1))^{\tau_{on}/2}$, corresponds to a power law. For a repulsive surface potential between the spheres, the forward step probability p_1 is reduced, and $P(\tau_{on},p_1)$ changes such that longer contact times occur less frequently, whereas shorter contact times are more likely. The single step probability $p_1(V)$ can be derived qualitatively from the interaction potential $V(r_{12})$, or can be obtained through Boltzmann statistics by the histogram of interparticle distances. It remains an interesting task how a non-linear interaction force translates into the distribution of contact times.

As shown in Fig. 4, the power law like behavior could be verified very well by our experimental results. Remarkably, the course of $P(\tau_{on},h)$ holds also for increased friction due to a decreased distance h to a surface. Whereas a nearby surface slows down the relative and collective particle diffusion, the distribution of contact times is hardly affected by the change in friction. This result is well described by our scale free formalism.

Hydrodynamic coupling to nearby interfaces

The hydrodynamic coupling of the spheres was analyzed in terms of cross-correlation functions (Fig. 8). In scanning direction, the particles motion is slowed down by a nearby wall and shows a positive correlation. In the perpendicular directions, the correlation functions reveal the anti-correlated behavior reported earlier.[5] A nearby surface strongly affects the particle motion for small distances. In this case, the mutual coupling is damped in comparison to the increase in friction and the negative dip in the correlation function attenuates.

This behavior is a result of differing diffusivities of the collective and relative particle motion. The diffusivities were determined experimentally in the vicinity of one and two confining surfaces for two particles in a single potential. For a single surface, the measurements agree well with theoretical predictions. However, in proximity of the second particle, the diffusivity of the first particle is reduced notably and the hydrodynamic coupling length $\Lambda(r_{12})$ is decreased significantly as shown by Fig. 6 and 7. Furthermore, a second nearby surface leads to even higher friction coefficients. The diffusivities of two particles in a chamber could be explained by a linear superposition principle and shows the qualitative expected behavior.

7. Conclusion

Hydrodynamic coupling is supposed to play a key role in biological processes, especially in particle interactions and binding probabilities in confined compartments[33] Whereas changes in viscous drag hardly affect the contact times and the binding probability between the particles, the diffusivity is reduced strongly. If the size of a cellular compartment is reduced to increase the binding probability of two particles therein, the increase in contact times is achieved simply by the reduced reaction volume pushing the particles together. The accompanying increased viscous drag simply slows down all processes in time. In this way less information per time can be transferred between particle and surface, *e.g.* through hydrodynamic momentum transfer.[34] We believe that our experimental results in combination with the theoretical framework can be used to explain reaction processes in more complex environments containing more complex particle distributions.

Acknowledgements

This study was supported by the Excellence Initiative of the German Federal and State Governments (EXC 294) and by the Deutsche Forschungsgemeinschaft (DFG), grant number RO 3615/1.

References

1 M. a. Nowak and H. Ohtsuki, Prevolutionary dynamics and the origin of evolution, *Proc. Natl. Acad. Sci. U. S. A.*, 2008, **105**, 14924–14927.

2 B. Alberts, *Essential Cell Biology*, Garland Science, 2010.
3 G. K. Batchelor, *An introduction to fluid dynamics*, 1998.
4 J. K. G. Dhont, *An Introduction to Dynamics of Colloids*, Elsevier, Amsterdam, 1996.
5 J. Meiners and S. R. Quake, Direct Measurement of Hydrodynamic Cross Correlations between Two Particles in an External Potential, *Phys. Rev. Lett.*, 1999, **82**, 2211–2214.
6 P. Bartlett, S. Henderson and S. Mitchell, Measurement of the hydrodynamic forces between two polymer-coated spheres, *Philos. Trans. R. Soc. London*, 2001, **359**, 883–895.
7 E. Schäffer, S. F. Norrelykke and J. Howard, Surface Forces and Drag Coefficients of Microspheres near a Plane Surface Measured with Optical Tweezers, *Langmuir*, 2007, **23**, 3654–3665.
8 L. P. Faucheux and A. J. Libchaber, Confined Brownian motion, *Phys. Rev. E: Stat., Nonlinear, Soft Matter Phys.*, 1994, **49**, 5158–5163.
9 E. Dufresne, D. Altman and D. Grier, Brownian dynamics of a sphere between parallel walls, *EPL*, 2001, **53**, 264–270.
10 E. R. Dufresne, T. M. Squires, M. P. Brenner and D. G. Grier, Hydrodynamic coupling of two brownian spheres to a planar surface, *Phys. Rev. Lett.*, 2000, **85**, 3317–3320.
11 M. Irmscher, A. M. De Jong, H. Kress and M. W. J. Prins, Probing the Cell Membrane by Magnetic Particle Actuation and Euler Angle Tracking, *Biophys. J.*, 2012, **102**, 698–708.
12 H. Kress, E. H. K. Stelzer, G. Griffiths and A. Rohrbach, Control of relative radiation pressure in optical traps: Application to phagocytic membrane binding studies, *Phys. Rev. E: Stat., Nonlinear, Soft Matter Phys.*, 2005, **71**, 061927.
13 A. Cervantes-Martínez, A. Ramírez-Saito, R. Armenta-Calderón, M. Ojeda-López and J. Arauz-Lara, Colloidal diffusion inside a spherical cell, *Phys. Rev. E: Stat., Nonlinear, Soft Matter Phys.*, 2011, **83**, 1–4.
14 X. Xu, S. a. Rice, B. Lin and H. Diamant, Influence of Hydrodynamic Coupling on Pair Diffusion in a Quasi-One-Dimensional Colloid System, *Phys. Rev. Lett.*, 2005, **95**, 158301.
15 G. M. Cicuta, J. Kotar, A. T. Brown, J.-H. Noh and P. Cicuta, Hydrodynamic coupling in polygonal arrays of colloids: Experimental and analytical results, *Phys. Rev. E: Stat., Nonlinear, Soft Matter Phys.*, 2010, **81**, 051403.
16 A. Zöttl and H. Stark, Hydrodynamics Determines Collective Motion and Phase Behavior of Active Colloids in Quasi-Two-Dimensional Confinement, *Phys. Rev. Lett.*, 2014, **112**, 118101.
17 L. Lobry and N. Ostrowsky, Diffusion of Brownian particles trapped between two walls: Theory and dynamic-light-scattering measurements, *Phys. Rev. B: Condens. Matter Mater. Phys.*, 1996, **53**, 12050–12056.
18 H. Diamant, B. Cui, B. Lin and S. a. Rice, Hydrodynamic interaction in quasi-two-dimensional suspensions, *J. Phys.: Condens. Matter*, 2005, **17**, S2787–S2793.
19 J. Happel and H. Brenner, *Low Reynolds Number Hydrodynamics. Englewood Cliffs NJ*, 1991, Kluwer Academic Publishers, vol. 40, pp. 1–553.
20 L. Friedrich and A. Rohrbach, Improved interferometric tracking of trapped particles using two frequency-detuned beams, *Opt. Lett.*, 2010, **35**, 1920–1922.
21 M. Speidel, L. Friedrich and A. Rohrbach, Interferometric 3D tracking of several particles in a scanning laser focus, *Opt. Express*, 2009, **17**, 7–9.
22 B. Tränkle, M. Speidel and A. Rohrbach, Interaction dynamics of two colloids in a single optical potential, *Phys. Rev. E: Stat., Nonlinear, Soft Matter Phys.*, 2012, **86**, 1–5.
23 D. Ruh, B. Tränkle and A. Rohrbach, Fast parallel interferometric 3D tracking of numerous optically trapped particles and their hydrodynamic interaction, *Opt. Express*, 2011, **19**, 1832–1835.
24 L. Friedrich and A. Rohrbach, Improved interferometric tracking of trapped particles using two frequency-detuned beams, *Opt. Lett.*, 2010, **35**, 1920–1922.
25 D. Ruh, B. Tränkle and A. Rohrbach, Fast parallel interferometric 3D tracking of numerous optically trapped particles and their hydrodynamic interaction, *America*, 2011, **021907**, 1832–1835.
26 P. Hilton and J. Pedersen, Catalan numbers, their generalization, and their uses, *Math. Intel.*, 1991, **13**, 65–75.
27 I. N. Bronstein, K. A. Semendjajew, G. Musiol and H. Mühlig, *Taschenbuch der Mathematik. Taschenbuch der Mathematik*, Verlag Harri Deutsch, 2001, vol. 23, p. 1216.
28 J. Wan and X. Xu, Pólya number and first return of bursty random walk: Rigorous solutions, *Physica A*, 2012, **391**, 1919–1927.
29 J.-C. Meiners and S. R. Quake, Direct Measurement of Hydrodynamic Cross Correlations between Two Particles in an External Potential, *Phys. Rev. Lett.*, 1999, **82**, 2211–2214.
30 H. Faxen, Dissertation, 1921.
31 G. K. Batchelor, Diffusion in a dilute polydisperse system of interacting spheres, *J. Fluid Mech.*, 1983, **131**, 155.
32 M. N. Skryabina, E. V. Lyubin, M. D. Khokhlova and A. A. Fedyanin, Probing of pair interaction of magnetic microparticles with optical tweezers, *JETP Lett.*, 2012, **95**, 560–564.
33 A. Fallah-Araghi, *et al.* Enhanced Chemical Synthesis at Soft Interfaces: A Universal Reaction-Adsorption Mechanism in Microcompartments, *Phys. Rev. Lett.*, 2014, **112**, 028301.
34 F. Jünger, *et al.* Measuring local viscosities near plasma membranes of living cells with photonic force microscopy, *Biophys. J.*, 2015, **109**, 869–882.

